Multiphoton microscopy for label-free multicolor imaging of peripheral nerve

Lars Rishøj[a,b,*,†] **Iván Coto Hernández**[c,*,†] **Siddharth Ramachandran**[a] **and Nate Jowett**[c]

[a]Boston University, Department of Electrical and Computer Engineering, Boston, Massachusetts, United States
[b]Technical University of Denmark, DTU Fotonik, Kgs. Lyngby, Denmark
[c]Mass Eye and Ear and Harvard Medical School, Surgical Photonics and Engineering Laboratory, Boston, United States

Abstract

Significance: Means for quantitation of myelinated fibers in peripheral nerve may guide diagnosis and clinical decision making in management of peripheral nerve disorders. Multiphoton microscopy techniques such as the third-harmonic generation enable label-free *in vivo* imaging of peripheral nerves.

Aim: Develop a multiphoton microscope based on a custom high-power infrared fiber laser for label-free imaging of peripheral nerve.

Approach: A cost-effective multiphoton microscope employing a single fiber laser source at 1300 nm was designed and used for stain-free multicolor imaging of murine and human peripheral nerve.

Results: Second-harmonic generation signal from collagen centered about 650-nm delineated neural connective tissue, whereas third-harmonic general signal centered about 433-nm delineated myelin and other lipids. In sciatic nerve from transgenic reporter mice expressing yellow fluorescent protein within peripheral neurons, three-photon-excitation with emission peak at 527-nm delineated axoplasm. The signal obtained from unlabeled axially sectioned samples was adequate for segmentation of myelinated fibers using commercial image processing software. In unlabeled whole mount specimens, imaging depths over 100-μm were achieved.

Conclusions: A multiphoton microscope powered by a fiber laser enables stain-free histomorphometry of mammalian peripheral nerve. The simplicity of the microscope design carries potential for clinical translation to inform decision making in peripheral nerve disorders.

 [DOI: 10.1117/1.JBO.27.5.056501]

Keywords: lasers; imaging; label-free; nonlinear optical microscopy; nerve fibers; myelinated.

Paper 210327GRR received Oct. 26, 2021; accepted for publication Apr. 13, 2022; published online May 16, 2022.

1 Introduction

Nonlinear optical microscopy (NLOM) comprises multiphoton fluorescence and harmonic generation techniques[1–3] that enable imaging of biologic tissue including peripheral nerve at depths far exceeding those achievable by single-photon excitation microscopy.[4,5] Label-free NLOM approaches for imaging peripheral nerve include coherent Raman scattering (CARS)[6] microscopy, second harmonic generation (SHG),[7,8] third harmonic generation (THG) microscopy,[9] or a combination of SHG and THG imaging.[10] Here, a custom-built fiber laser based on soliton self-mode conversion (SSMC)[11] is employed for multi-color and high-resolution NLOM[12] of murine and human peripheral nerve.[13,14] Collagen is a primary constituent of the peripheral nerve

*Address all correspondence to Iván Coto Hernández, ivan_cotohernandez@meei.harvard.edu; Lars Rishøj, lris@fotonik.dtu.dk
†These authors contributed equally to the work.

sheath and extracellular matrix encasing individual axons; dysregulation in collagen production impacts nerve regeneration.[15,16] Myelin is a lipid-rich substance that envelops select central and peripheral nervous system axons, providing mechanical protection and electrical insulation for rapid and efficient propagation of action potentials. Dysregulation of myelin production is a hallmark of manifold neurological disease states.[17] In this paper, peripheral nerve sheaths, myelin sheaths, and individual axons are imaged using a custom single excitation source within the second optical window (~1300 nm).[18] Collagen-dense nerve sheaths (endoneurium, perineurium, and epineurium) are resolved using an SHG signal centered at ~650 nm, whereas lipid-dense myelin sheaths of individual myelinated axons are resolved using a THG signal centered at ~433 nm. Additionally, excitation wavelengths around 1300-nm enable 3PE of popular green and yellow fluorescent proteins [green fluorescent protein (GFP) and yellow fluorescent protein (YFP)][19] and two-photon excitation of several red-fluorescent-dyes.[20] Here, stain-free multicolor imaging of peripheral nerve from transgenic mice expressing YFP under control of a modified thy1 promoter is achieved with capture of YFP emission maximum at 527 nm delineating the axoplasm of individual axons, and SHG and THG signals delineate neural connective tissue and myelin sheaths, respectively.

2 Experimental Setup and Biological Samples

A custom multiphoton microscope for multicolor imaging of peripheral nerve was designed and assembled. A custom fiber laser system based on SSMC with a tunable wavelength range from 1045 to 1320 nm was optimized at a single wavelength (~1300 nm), selected to minimize biological sample damage while allowing for deep NLOM imaging. The experimental setup is shown in Fig. 1. It consists of three elements, the laser system (blue shaded region),

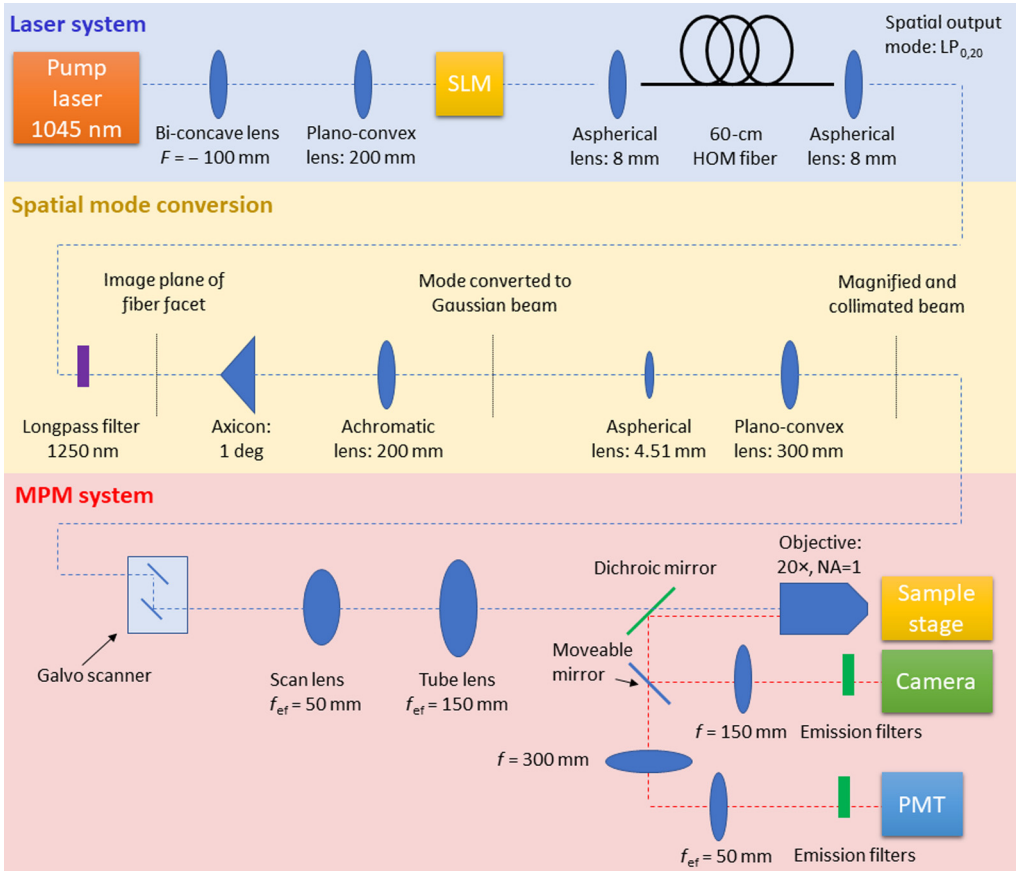

Fig. 1 Experimental setup. The hardware employed comprises the laser system (blue shaded region), spatial mode conversion (yellow shaded region), and the MPM system (red shaded region).

spatial mode conversion (yellow shaded region), and the multiphoton microscopy (MPM) system (red shaded region), which are described below. More information about the laser system and spatial mode conversion can be found in Refs. 11 and 21.

2.1 *Laser System*

The blue shaded region of Fig. 1 is the laser system, where a 100 fs pulse at 1045 nm from the pump laser (Y-Fi, KMLabs, Boulder, Colorado, United States) is converted to ∼1300 nm. A telescope magnifies the beam before propagation onto a spatial light modulator, which encodes a transverse spatial phase onto the incident Gaussian beam to ensure excitation of a single pure mode in the multimode fiber.[21] Here, a linearly polarized (LP) $(LP)_{0,21}$ mode is excited in the custom 54-cm higher-order-mode fiber (core diameter of 97 μm and numerical aperture of 0.34). Initially in the fiber, a soliton is formed at the pump wavelength in the $LP_{0,21}$ mode and subsequently the center wavelength of the soliton continuously red-shifts via soliton self-frequency shifting (SSFS). The soliton eventually reaches a wavelength at which it has the same group velocity as the $LP_{0,20}$ mode at a longer wavelength that is separated by a frequency detuning equal to the Raman gain peak of silica (13 THz). At this point, the energy of the soliton is transferred via the recently discovered nonlinear effect of SSMC to a new pulse in the $LP_{0,20}$ mode. From this point, until the end of the fiber, the new pulse then frequency shifts via SSFS to 1317 nm where the pulse energy is measured to be 80 nJ.[11,22] Figure 2(a) shows the output spectra from the fiber before and after spectral filtering with a 1250-nm longpass filter. Figure 2(b) shows the spatial mode of the pulse centered at 1317 nm. It is seen to be in the $LP_{0,20}$ mode, which resembles a truncated Bessel beam comprising a central peak surrounded by 19 concentric rings. This exact frequency conversion process requires that light initially possessed certain linear properties, which is ensured by launching the light in a specific higher order mode in the multimode fiber, which in this case is the $LP_{0,21}$ mode. Using an autocorrelator, the pulse duration was measured at 74 fs, corresponding to a peak power of ∼1.1 MW. Based on the measured spectral bandwidth, it was found that the pulses are nearly transform-limited, an expected result considering the pulses are solitons.

2.2 *Spatial Mode Conversion*

In the yellow shaded region of the experimental setup shown in Fig. 1, a longpass filter initially removes the residual pump light. Next, the $LP_{0,20}$ fiber output mode is converted to a Gaussian-like beam using an axicon and lens, with a measured power conversion efficiency of 81% (theoretically 86%).[11] Figure 2(c) shows the image of the Gaussian beam after the spatial mode conversion. The following two lenses magnify and collimate the Gaussian beam to a beam diameter of 5 mm [full width at half maximum (FWHM)]. At this point, the pulse duration was measured at 100 fs using an autocorrelator. Though Bessel beams may be used to extend the depth of focus and for fast volumetric imaging of sparse samples,[19] a Gaussian beam was utilized as it is more energy-efficient for imaging histological sections of excised nerves.

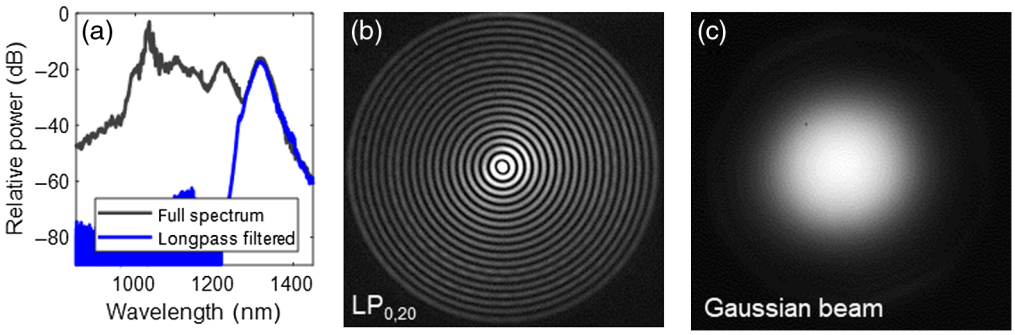

Fig. 2 (a) Output spectrum before and after spectral filtering. (b) Experimental image of the $LP_{0,20}$ output mode after spectral filtering. (c) Gaussian beam after spatial re-conversion.

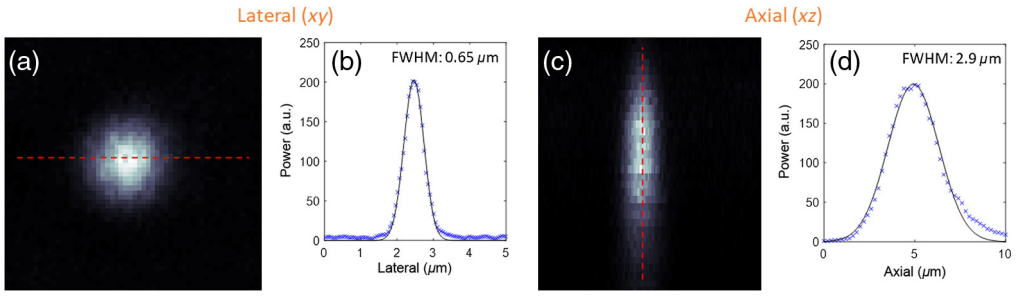

Fig. 3 PSF measurements. (a) The lateral FWHM is 0.65 μm. (b) The axial FWHM is 2.9 μm.

2.3 *Multiphoton Microscope*

The multiphoton microscope is shown in the red shaded region of Fig. 1. The system was designed de novo around the aforementioned 1300-nm fiber laser, for cost efficiency and performance optimization. Galvo mirrors (GVS002, Thorlabs, Newton, New Jersey, United States) are used to scan the beam. The scan and tube lenses comprise of several air-spaced commercial lenses from Thorlabs. The optical design was optimized in Zemax to minimize aberrations, resulting in diffraction-limited performance for optical ray angles below 11.3 deg. The scan lens consists of two LA1541-C lenses and a LA1031-C lens and the tube lens consists of two AC508-300-C. The signals are epi-collected by a 20× (NA = 1) objective lens (XLUMPLFLN20XW, Olympus, Tokyo, Japan), separated by a 775-nm longpass dichroic mirror (FF775-Di01, Semrock Inc., Rochester, New York, United States), and then detected sequentially using emission filters by a photomultiplier tubes (PMT) (H7422-40, Hamamatsu Photonics, Hamamatsu, Japan). The collection path was designed in Zemax from commercial lenses (Thorlabs) to ensure maximum collection efficiency. The first lens (Thorlabs LA1256-A) is followed by an air-spaced lens consisting of three plano-convex lenses (Thorlabs LA1417-A). This optical design ensures a full collection field-of-view (FOV) of ∼1 mm in diameter. The sample stage enabled coarse lateral movement and axial scanning using a three-dimensional (3D) stepper motor (TRA25CC, Newport Corp., Irvine, California, United States). A moveable silver mirror downstream of the dichroic mirror enables optional widefield imaging. The pre-amp is a FEMTO DHPCA-100 (FEMTO Messtechnik GmbH, Berlin, Germany), and the data acquisition card is an NI PCIe-6353 (National Instruments Corp., Austin, Texas, United States). Samples were excited using the same wavelength and pulse duration, but images were sequentially collected beginning with the signal requiring the least pulse energy (i.e., SHG) to minimize the risk of photodamage. The power was adjusted using a combination of neutral density filters, and polarization control was employed to maximize the signal strength. Images were collected with specific bandpass-filters to isolate SHG, THG, and 3PE fluorescence signals. Through the appropriate choice of filters crosstalk between images was avoided, as evident from the signals being delocalized between the images. The power dependency of the three signals was verified by collecting emission as a function of illumination beam power. The microscope system was controlled using ScanImage and the images were processed using ImageJ software (Fiji Distribution, Version 1.52e).[23,24] Frame averaging was used to further minimize noise. Colors were arbitrarily assigned to the grayscale images. The pulse duration was measured using an autocorrelator after the objective lens at 114 fs. The point spread function (PSF) of the system was measured using 175-nm blue fluorescent beads; the results for the lateral (0.65 μm) and axial (2.9 μm) directions are shown in Fig. 3. For calibration and PSF measurements, the fiber laser was operated at a repetition rate of 1 MHz. For biological sample imaging, the repetition rate of the laser was increased to 10 MHz to improve scanning efficiency. In both instances, the maximum pulse energy at the sample plane was ∼10 nJ.

A summary of the optical performance of the MPM system is given in Table 1.

2.4 *Biological Samples*

Experimental protocols were approved by the Mass Eye and Ear Internal Review Boards, and all methods were carried out in accordance with relevant guidelines and regulations. Fresh frozen

Table 1 Performance of MPM system.

Specification	Value
Wavelength	~1300 nm
Maximum pulse energy (post objective)	10 nJ
Pulse duration (post objective)	114 fs
Maximum peak power (post objective)	87 kW
Maximum average power (post objective)	100 mW
Repetition rate	10 MHz
MPM system loss	6.6 dB
Lateral PSF (FWHM)	0.65 μm
Axial PSF (FWHM)	2.9 μm
FOV	1 × 1 mm
Spatial mode	Gaussian

sections of healthy human motor branch of obturator nerve and transgenic mice sciatic nerve were employed. Adult human nerve samples (patient age >18 years) were obtained fresh at the time of the free-tissue transfer for smile reanimation after informed consent among patients undergoing facial reanimation procedures. Sciatic nerves from thy1-YFP mice were harvested in accordance with Massachusetts Eye and Ear Institutional Animal Care and Use Committee approval. Specifically, animals were placed in an induction chamber and placed under general anesthesia by inhalation of 2% isoflurane in 0.6 l/ min O_2. Once unconscious, isoflurane was increased to 5% and continued until cessation of breathing was noted for one minute, followed by immediate cervical dislocation. Nerves were immediately harvested from the carcasses. Whole mounts were kept at 4°C in saline-soaked gauze and imaged fresh within 2 h. Nerves for sectioning were processed using a previously described protocol.[25] Briefly, nerves were fixed by immersion in 2% phosphate-buffered paraformaldehyde, followed by cryoprotection in sucrose solution, cryosectioning at 1 to 2 μm, and staining using a non-toxic myelin-specific dye followed by mounting on glass slides prior to multiphoton imaging.

3 Experimental Results

System performance and laser parameters including PSF, pulse energy, and duty cycle were optimized to enhance image contrast and acquisition time while minimizing photodamage. The use of 1300 nm permits simultaneous multiphoton excitation and multiharmonic generation microscopy while avoiding undesirable two-photon absorption from endogenous fluorophores (namely, NADH and FAD), with subsequent cross-talk and photodamage.

3.1 *Imaging of Human Obturator Nerve*

The microscope was used for SHG and THG epi-detection imaging of human and murine peripheral nerve. Figures 4(a) and 4(b) show images of axially frozen-sectioned human obturator nerve obtained sequentially with different bandpass filters (BPF). For this label-free sample, the SHG signal (617/73 nm BPF) was generated from collagen in the three nerve sheath layers (endoneurium, perineurium, and epineurium). Collagen is the main tissue component responsible for an SHG signal in peripheral nerve tissue. For validation of label-free SHG imaging, picrosirius red was employed on separate tissue sections as an efficient alternative to immunohistochemistry for high-specificity labeling of collagen-dense structures. Picrosirus red-stained collagen was imaged using brightfield microscopy[26] as shown in Fig. 4(c). A THG signal (420/50-nm BPF) was predominately generated from the myelin sheaths of myelinated axons [Fig. 4(b)],

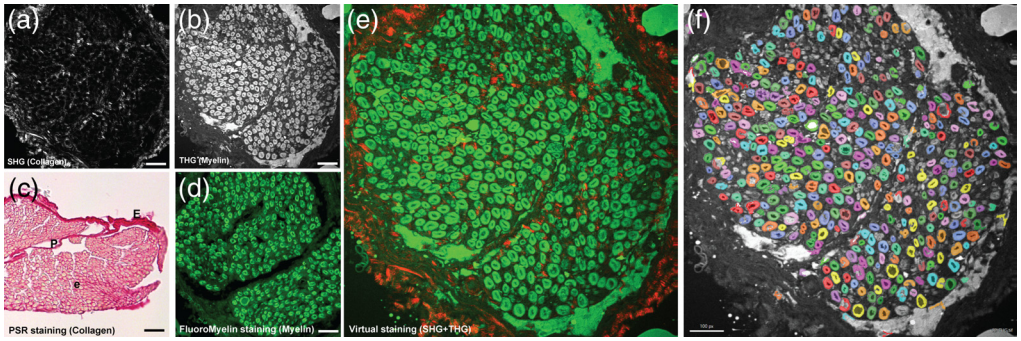

Fig. 4 Label-free imaging of *ex vivo* human obturator nerve cross-sections using a novel 1300-nm fiber laser-powered multiphoton microscope. (a) Second-harmonic generation imaging of neural connective tissue collagen, post objective average power 7.5 mW. (b) Third-harmonic generation imaging of myelinated fibers, post objective average power 15 mW. (c) Picrosirius red staining of myelinated fibers (conventional light microscopy). (d) Myelin-specific dye (FluoroMyelin Green, Molecular Probes, Eugene, Oregon, United States) staining of cross-section (widefield fluorescence microscopy). (e) Merged image combining SHG (red) and THG (green) signals. (f) Automated histomorphometry of peripheral nerve human obturator nerve section imaged by THG. The FOV is 380×380 μm, and the scale bar is 50 μm.

demonstrating near-identical imaging results compared to widefield fluorescence imaging of myelin-specific dye stained sections, as shown in Fig. 4(d). Though the THG signal is predominantly emitted in the forward direction, there is sufficient backward-scattering in turbid media (such as peripheral nerve) to obtain a sufficient signal using epi-detection as demonstrated here and by other groups.[9,27] The combination of photobleaching-free SHG and THG images reveal complementary information allowing characterization of nerve morphology in unstained tissues, as shown in Fig. 4(e). Figure 4(f) shows myelinated axon quantification of unlabeled cryosectioned human peripheral nerve performed through segmentation of a THG image using commercial machine learning software.[28]

3.2 *Imaging of Sciatic Murine Nerve*

Figure 5 shows imaging of a sciatic nerve cross-section from a thy1-YFP mouse using the multiphoton microscope developed here. Three-photon-excitation fluorescence images were collected using a third filter (535/60 nm BPF) to separate them from SHG and THG signals. Figures 5(a)–5(c) show a THG signal from myelin, SHG signal from collagen, and three-photon fluorescence excitation signal from YFP-labeled axons. In Fig. 5(d), the three images are merged to obtain a multicolor image.

To estimate the nonlinear order and required power for multiphoton imaging, the dependence of the signal on excitation power was measured. The plot of signal strength versus excitation power is shown in Fig. 6, along with fits. The black-dashed lines represent the power order as a free-fitting parameter, and the red-dashed lines represent fits with fixed power order. The fits show excellent agreement with the data, indicating capture of appropriate emission. Excitation power exhibits a second-order increase in the SHG signal (×1.90) and third-order increase in the 3PE (×2.99) and THG (×3.24) signals.

To assess whether this novel 1300-nm fiber-based multiphoton microscope could potentially be employed for *in vivo* imaging of mammalian nerve, freshly harvested whole mount murine sciatic nerve from a thy1-YFP mouse was imaged. Figure 7 shows the results for 3PE [Fig. 7(a), YFP] and THG imaging [Fig 7(b), myelin] using non-descanned epi-detection at a depth of 120 μm into the tissue. The two images are merged in Fig. 7(c).

4 Discussion

Disorders of myelination are cardinal features of several inherited and acquired diseases of the nervous system.[17] Noninvasive neuroimaging techniques based on magnetic resonance imaging

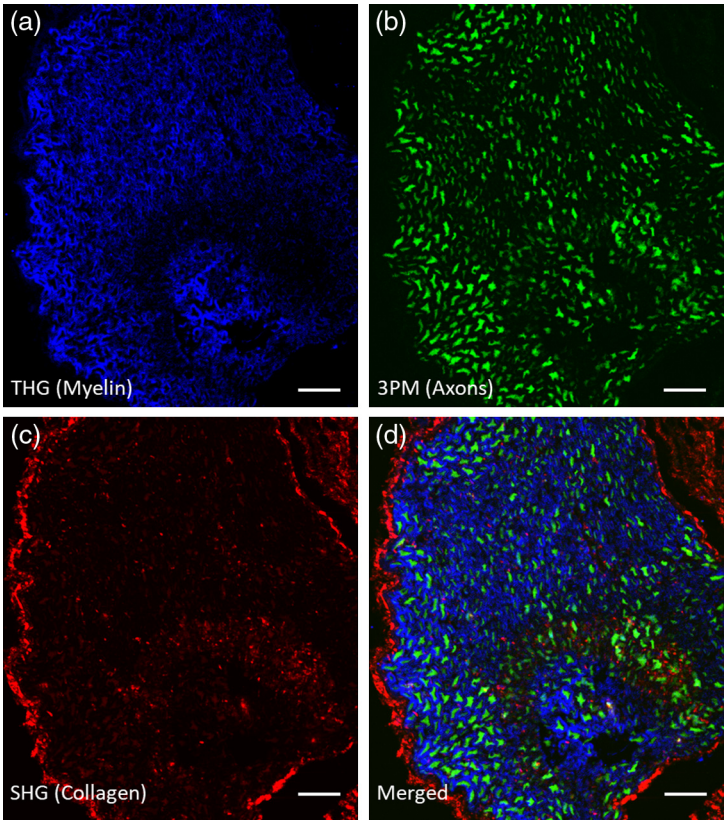

Fig. 5 Multiphoton-microscopy image of *ex vivo* sciatic nerve of a thy1-YFP mouse. FOV is 210×240 μm. Scale bars are 25 μm. Post objective average power was 12.5 mW. (a) Third-harmonic generation (blue) shows the myelinated fibers. (b) Three-photon excited fluorescence of YFP (green) shows axons. (c) Second-harmonic generation (red) shows collagen fibers. (d) Merged image of THG, 3PE, and SHG signals.

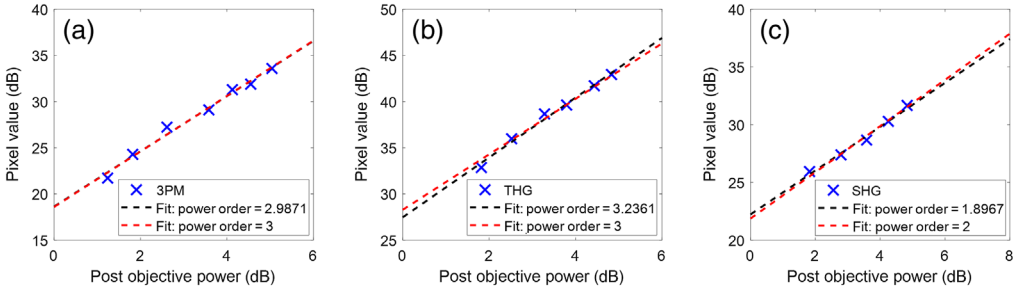

Fig. 6 Power dependence of the three signals measured in Fig. 5. (a) Three-photon signal. (b) THG signal. (c) SHG signal.

are useful for diagnosis and monitoring of several demyelinating diseases,[29] but lack resolution necessary for quantitation of individual fibers. In surgery for peripheral nerve dysfunction, means for rapid and reliable quantification of axons present within nerve branches could inform operative decision making.[30–33] The present study demonstrated the potential of label-free multiphoton microscopy paired with rapid cryosection techniques for quantitation of myelinated axons in human nerve relevant to clinical practice. In peripheral nerves of transgenic reporter mice, stain-free multicolor imaging epineurial sheaths, unmyelinated and myelinated axons were achieved using a single excitation wavelength, demonstrating the utility of this microscopy platform as a research tool.

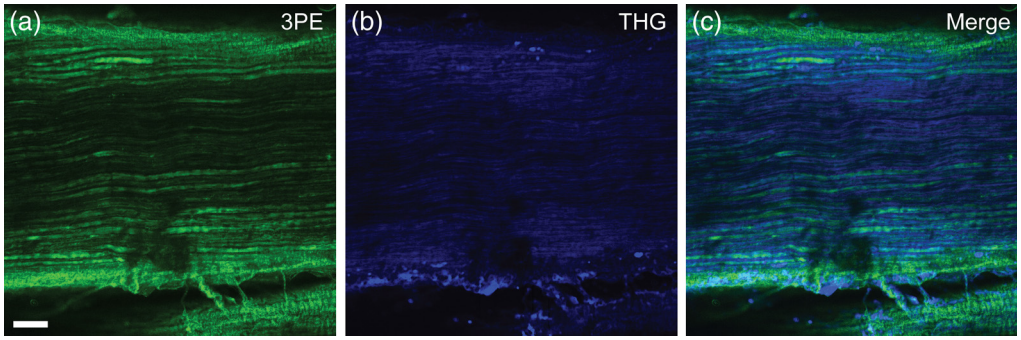

Fig. 7 Multiphoton-microscopy images of wet mounted sciatic nerve of a thy1-YFP mouse at a depth of 120 μm, post objective average power was 30 mW. (a) Three-photon excited fluorescence of YFP (green) shows axons. (b) Third-harmonic generation (blue) signal shows the myelinated fibers. (c) Merged image of 3PE and THG signals. About 50 frame averages were used to enhance image quality. FOV is 480×480 μm. Scale bars is 50 μm.

Nerve histomorphometry based on conventional axial sectioning approaches necessitates nerve biopsy, yielding loss of neural function. A key advantage of THG microscopy over other high-resolution imaging techniques is its potential for resolution of individual myelinated fibers within intact peripheral nerve, as has been previously demonstrated using an 1180-nm laser illumination source.[9] Though THG imaging of central nervous system tissue has been achieved at depths up to a few hundred microns, imaging of peripheral axons in intact peripheral nerve is challenging owing to the highly scattering properties of the epineurial sheath. Heretofore, two-photon excitation imaging of myelinated axons within intact mammalian peripheral nerve has been limited depths <70 μm.[34] Here, we achieved an imaging depth exceeding 100 μm within intact excised peripheral nerve using 3PE at 1300 nm. In comparison to illumination below 1200 nm, longer illumination wavelengths for THG imaging yields longer wavelength emission in the visible (>400 nm) as opposed to ultraviolet (<400 nm) domains, lessening undesirable signal absorption to permit deeper imaging. Longer illumination wavelengths also increase achievable imaging depth of SHG of collagen.[35]

Several commercial femtosecond lasers exist with outputs at 1300 nm. However, these lasers may lack the necessary peak power to achieve THG. As shown in the Supplementary Materials, additional sections were imaged using a commercial multiphoton microscope. Despite identical PMT and BPF and similar epi-collection non-descanned optical paths, insufficient signal was captured to resolve THG and 3PE signals (Fig. S1 in the Supplementary Materials).

Future work will examine means to optimize lateral and axial resolution in multiphoton microscopy. An epi-detection NLOM imaging signal is typically collected via non-descanned detection, using a large area detector positioned close to the objective lens to minimize signal loss along the collection path. Alternatively, descanned confocal detection may potentially be employed to minimize background signal and increase axial resolution, though loss of signal along the descanned detection path and pinhole may negate potential gains in the signal-to-background ratio. In place of a pinhole and single point detector, an array of photodetectors (e.g., Zeiss Airyscan detector, Carl Zeiss AG, Jena Germany) paired with deconvolution algorithms could be alternatively employed to optimize a descanned detection signal by capturing photons that would otherwise be discarded by the pinhole.[36] Spatial resolution could be further enhanced by digital pixel reassignment or blind image reconstruction, as previously reported for two-photon emission microscopy.[37,38]

5 Conclusion

We developed a novel microscope based on a custom-built 1300-nm excitation source for multi-harmonic and multi-photon excitation microscopy. We demonstrated the utility of the microscope in label-free imaging of intact peripheral nerves and frozen sections of healthy murine sciatic nerve and healthy human obturator nerve. Three-photon fluorescence, SHG, and THG

imaging were achieved using a cost-efficient custom fiber-based high-powered near-infrared femtosecond laser source. Despite a long illumination wavelength at 1300 nm, an adequate SHG signal to highlight collagen-rich endoneurium, perineurium, and epineurium was obtained via non-descanned epi-detection. The combination of SHG and THG imaging using a novel single fiber femtosecond laser source at 1300 nm represents means for label-free imaging of peripheral nerve with potential clinical implications for non-ablative neural histomorphometry.

Disclosures

The authors have no relevant financial interests in the manuscript and no other potential conflicts of interest to disclose.

Acknowledgments

The authors would like to thank Anderson Chen (Boston University) for helping with Zemax simulations and Suresh Mohan (Mass Eye and Ear) for sample preparation. A portion of this work was supported by the National Institute of Neurological Disorders and Stroke of the National Institutes of Health under award number R01NS071067 and by a generous donation from the Berthiaume Family. The work was also funded by National Institute of Health (Grant No. 1R21EY026410-01), Air Force Office of Scientific Research (Grant No. FA9550-14-1-0165), and Office of Naval Research (Grant No. N00014-17-1-2519).

Code, Data, and Materials Availability

Code and data can be made available upon request to the corresponding author.

References

1. D. Débarre et al., "Imaging lipid bodies in cells and tissues using third-harmonic generation microscopy," *Nat. Methods* **3**(1), 47–53 (2006).
2. R. Genthial et al., "Label-free imaging of bone multiscale porosity and interfaces using third-harmonic generation microscopy," *Sci. Rep.* **7**, 3419 (2017).
3. S. You et al., "Intravital imaging by simultaneous label-free autofluorescence-multiharmonic microscopy," *Nat. Commun.* **9**, 2125 (2018).
4. W. Denk, J. H. Strickler, and W. W. Webb, "Two-photon laser scanning fluorescence microscopy," *Science* **248**(4951), 73–76 (1990).
5. A. Diaspro, G. Chirico, and M. Collini, "Two-photon fluorescence excitation and related techniques in biological microscopy," *Q. Rev. Biophys.* **38**(2), 97–166 (2005).
6. C. W. Freudiger et al., "Label-free biomedical imaging with high sensitivity by stimulated Raman scattering microscopy," *Science* **322**(5909), 1857–1861 (2008).
7. H. Lim and J. Danias, "Effect of axonal micro-tubules on the morphology of retinal nerve fibers studied by second-harmonic generation," *J. Biomed. Opt.* **17**(11), 110502 (2012).
8. E. B. Sinclair et al., "Relating applied strain to the type and severity of structural damage in the rat median nerve using second harmonic generation microscopy," *Muscle Nerve* **46**(6), 895–898 (2012).
9. H. Lim et al., "Label-free imaging of Schwann cell myelination by third harmonic generation microscopy," *Proc. Natl. Acad. Sci.* **111**(50), 18025–18030 (2014).
10. S. Chakraborty et al., "Additive-color multi-harmonic generation microscopy for simultaneous label-free differentiation of plaques, tangles, and neuronal axons," *Biomed. Opt. Express* **11**(2), 571–585 (2020).
11. L. Rishøj et al., "Soliton self-mode conversion: revisiting Raman scattering of ultrashort pulses," *Optica* **6**(3), 304–308 (2019).
12. L. Rishaj et al., "Multiharmonic imaging of human peripheral nerves using a 1300 nm ultrafast fiber laser," in *CLEO: Appl. and Technol.*, ATh3K.2 (2020).

13. J. P. Zinter and M. J. Levene, "Maximizing fluorescence collection efficiency in multiphoton microscopy," *Opt. Express* **19**(16), 15348–15362 (2011).
14. M. Yildirim et al., "Functional imaging of visual cortical layers and subplate in awake mice with optimized three-photon microscopy," *Nat. Commun.* **10**, 177 (2019).
15. P. Chen et al., "Collagen VI regulates peripheral nerve myelination and function," *FASEB J* **28**(3), 1145–1156 (2014).
16. G. Koopmans, B. Hasse, and N. Sinis, "The role of collagen in peripheral nerve repair," *Int. Rev. Neurobiol.* **87**, 363–379 (2009).
17. I. D. Duncan and A. B. Radcliff, "Inherited and acquired disorders of myelin: the underlying myelin pathology," *Exp. Neurol.* **283**, 452–475 (2016).
18. A. M. Smith, M. C. Mancini, and S. Nie, "Second window for *in vivo* imaging," *Nat. Nanotechnol.* **4**(11), 710–711 (2009).
19. B. Chen et al., "Rapid volumetric imaging with Bessel-beam three-photon microscopy," *Biomed. Opt. Express* **9**(4), 1992–2000 (2018).
20. T. Wang et al., "Three-photon imaging of mouse brain structure and function through the intact skull," *Nat. Methods* **15**(10), 789–792 (2018).
21. J. Demas, L. Rishøj, and S. Ramachandran, "Free-space beam shaping for precise control and conversion of modes in optical fiber," *Opt. Express* **23**(22), 28531–28545 (2015).
22. L. Rishøj et al., "Characterization of intermodal group index matched soliton interactions leading to MW peak powers at 1300 nm," in *CLEO: Sci. and Innovations*, STh3K. 2 (2017).
23. J. Schindelin et al., "Fiji: an open-source platform for biological-image analysis," *Nat. Methods* **9**(7), 676–682 (2012).
24. C. A. Schneider, W. S. Rasband, and K. W. Eliceiri, "NIH Image to ImageJ: 25 years of image analysis," *Nat. Methods* **9**(7), 671–675 (2012).
25. W. Wang et al., "A rapid protocol for intraoperative assessment of peripheral nerve myelinated axon count and its application to cross-facial nerve grafting," *Plast. Reconstructive Surg.* **143**(3), 771 (2019).
26. K. A. Wegner et al., "Fluorescence of picrosirius red multiplexed with immunohistochemistry for the quantitative assessment of collagen in tissue sections," *J. Histochem. Cytochem.* **65**(8), 479–490 (2017).
27. D. Débarre, N. Olivier, and E. Beaurepaire, "Signal epidetection in third-harmonic generation microscopy of turbid media," *Opt. Express* **15**(14), 8913–8924 (2007).
28. I. Coto Hernandez et al., "Label-free histomorphometry of peripheral nerve by stimulated Raman spectroscopy," *Muscle Nerve* **62**(1), 137–142 (2020).
29. J.-M. Tillema and I. Pirko, "Neuroradiological evaluation of demyelinating disease," *Ther. Adv. Neurol. Disorder* **6**(4), 249–268 (2013).
30. A. H. MacQuillan and A. O. Grobbelaar, "Functional muscle transfer and the variance of reinnervating axonal load: Part I. The facial nerve," *Plast. Reconstructive Surg.* **121**(5), 1570–1577 (2008).
31. A. H. MacQuillan and A. O. Grobbelaar, "Functional muscle transfer and the variance of reinnervating axonal load: part II. Peripheral nerves," *Plast. Reconstructive Surg.* **121**(5), 1708–1715 (2008).
32. J. K. Terzis, W. Wang, and Y. Zhao, "Effect of axonal load on the functional and aesthetic outcomes of the cross-facial nerve graft procedure for facial reanimation," *Plast. Reconstructive Surg.* **124**(5), 1499–1512 (2009).
33. A. Hembd et al., "Facial nerve axonal analysis and anatomical localization in donor nerve: optimizing axonal load for cross-facial nerve grafting in facial reanimation," *Plast. Reconstructive Surg.* **139**(1), 177–183 (2017).
34. A. K. Fontaine et al., "Deep-tissue two-photon imaging in brain and peripheral nerve with a compact high-pulse energy ytterbium fiber laser," *Proc. SPIE* **10492**, 1049217 (2018).
35. M. Balu et al., "Effect of excitation wavelength on penetration depth in nonlinear optical microscopy of turbid media," *J. Biomed. Opt.* **14**(1), 010508 (2009).
36. J. Huff et al., "Airyscan detection in multiphoton microscopy: super-resolution and improved signal-to-noise ratio beyond the confocal depth limit," *Nat. Methods* (2018).
37. C. J. Sheppard et al., "Image formation in image scanning microscopy, including the case of two-photon excitation," *J. Opt. Soc. Am. A* **34**(8), 1339–1350 (2017).

38. S. V. Koho et al., "Two-photon image-scanning microscopy with SPAD array and blind image reconstruction," *Biomed. Opt. Express* **11**(6), 2905–2924 (2020).

Lars Rishøj studied applied physics at Technical University of Denmark. He then worked as a postdoc and senior scientist at Boston University. Currently, he is a senior researcher at Technical University of Denmark. His research interest includes nonlinear fiber optics and higher order modes in optical fibers.

Iván Coto Hernández studied nanoscience at Italian Institute of Technology (Italy) in 2015. Currently, he serves as an instructor of otolaryngology—head and neck surgery, at Harvard Medical School. He has authored more than 25 journal papers. His current research interests include super-resolution and multiphoton microscopy. He is a member of SPIE.

Siddharth Ramachandran started his career at Bell Labs, and after a decade in industrial research labs, returned to academia, to Boston University, where he is currently a distinguished professor of engineering. His fields of interests include fundamental studies and applications of singular and spatiotemporally complex light. He is a fellow of SPIE, Optica (formerly OSA), and IEEE, and his awards include an IEEE Distinguished Lectureship and a Vannevar Bush Faculty Fellowship.

Nate Jowett studied medicine at the University of Toronto and obtained a PhD in biomedical engineering at McGill University. He serves as an assistant professor of otolaryngology—head and neck surgery, at Harvard Medical School. He has authored over 75 peer-reviewed papers. His research is focused on advancing knowledge and outcomes in the field of motor and sensory deficits of the head and neck.